

Implementing Shor's algorithm on Josephson Charge Qubits

Juha J. Vartiainen,^{1,*} Antti O. Niskanen,² Mikio Nakahara,^{1,3} and Martti M. Salomaa¹

¹*Materials Physics Laboratory, POB 2200 (Technical Physics),
FIN-02015 HUT, Helsinki University of Technology, Finland*

²*VTT Information Technology, Microsensing, POB 1207, 02044 VTT, Finland*

³*Department of Physics, Kinki University, Higashi-Osaka 577-8502, Japan*

(Dated: December 19, 2019)

We investigate both the physical and algorithmic requirements for an implementation of Shor's factorization algorithm on a hypothetical Josephson charge qubit register. We study an implementation which is optimal when only a small number of qubits is available, but still providing a universal method to factorize composite number of any size. In order to meet the stringent requirements set by a short decoherence time, we accelerate the algorithm by decomposing the quantum circuit into tailored two- and three-qubit gates and find their physical realizations through numerical optimization. This strategy is easily generalized to other physical realizations as well.

PACS numbers: 03.67.Lx, 03.75.Lm

Keywords: quantum computation, Josephson effect

I. INTRODUCTION

Any physical two-state quantum system that enables sufficient control and measurability over superposed states can, in principle, be treated as a quantum bit — a qubit. Many, widely different [1], physical systems serve to fulfill these criteria but yet the construction of a multiqubit register, large enough to act as a quantum computer, remains extremely challenging. Recently, remarkable progress has been accomplished for instance with nuclear spins [2, 3], trapped ions [4, 5], cavity quantum electrodynamics [6], electrons in quantum dots [7], and superconducting circuits [8, 9, 10, 11, 12, 13].

The characteristic properties of a quantum register, namely its coherence time, scalability, controllability, and integrability strongly depend on the particular realization. The largest quantum register thus far, comprising seven qubits, has been demonstrated with nuclear magnetic resonance (NMR) in a liquid solution [3]. However, the NMR technique is not believed to be scalable for much larger registers. In this paper we consider superconducting Josephson-junction circuits, which are supposed to be more feasible for large quantum registers since they not only allow an integration of the control and measurement electronics but also possibly enable good scalability [14]. A Josephson-junction circuit provides a two-state pseudospin system whose different spin components correspond to distinct macroscopic variables, namely either the charge on the superconducting island or the phase difference over a Josephson junction. Thus, depending on the parameter values for the setup, one has flux [8, 9], or charge qubits [10, 11, 12, 13, 15]. In this paper, we consider a hypothetical inductively coupled charge-qubit model [16].

In addition to the quantum register, one must have

techniques to implement a quantum algorithm. These involve: (1) a universal quantum compiler which transforms any abstract quantum algorithm X into a sequence of quantum gates $U_X = U_1 U_2 \cdots U_l$ which realizes the algorithm and (2) the quantum-gate library which contains information about the gate-operations available on the quantum computer. The resulting quantum circuit is similar to the operational principle of a conventional digital computer. In the standard approach the gate library consists of a set of universal elementary gates [17], which are typically chosen to be the one-qubit unitary rotations and the CNOT gate. The circuit, provided by the quantum compiler, can be optimized using various methods similar to those in digital computing [18], but yet the number of gates in the decomposition may be enormous. We have shown earlier [19] that if the gate library includes tailored two-, three- or any k -qubit gates, which we hereafter refer as modules, the quantum circuits may be made more compact. For further discussion of the utilization of tailored non-standard modules as the building blocks for quantum circuits, see Refs. [20, 21, 22].

The quantum-mechanical Hilbert space for an n -qubit quantum register is isomorphic with the space \mathbb{C}^{2^n} . Hence any n -qubit quantum algorithm X can be represented with a $2^n \times 2^n$ unitary matrix, U_X . The task to implement the desired algorithm X by directly finding the elements of the unitary matrix U_X and then the corresponding gate sequence scales exponentially with the size n of the register, which makes this approach intractable if n is large. Fortunately, efficient quantum gate decompositions are known for the most celebrated quantum algorithms, which include Shor's integer-factorization algorithm [23], Grover's database search [24], and the quantum error-correction codes [25, 26]. In this paper we consider integer factorization.

Quantum computation requires total control of the quantum state of the qubit register which poses a great experimental challenge. Moreover, a quantum register is never totally isolated from its environment since the

*Electronic address: juhav@focus.hut.fi

quantum-state preparation, manipulation and measurement must be performed during the execution of the quantum algorithm. The very many degrees of freedom of the environment tend to become entangled with those of the qubit register which results in undesirable decoherence [27]. Decoherence tends to destroy the quantum state which is needed for the quantum-information processing and, therefore, imposes a limit to the execution time available for the algorithm. These obstacles become even more pronounced when the size of the quantum register is increased. Eventually, they may present fundamental difficulties in scaling the quantum register up into large sizes, which is the basic requirement for the realization of reasonable quantum algorithms [28]. This also holds for Josephson-junction qubits; the strong coupling to the environment through the electrical leads [29] causes short decoherence times.

This paper is organized as follows: Section II discusses the implementation of Shor's factorization algorithm using a longhand multiplication scheme. Consequently, a large number of qubits and modules is required compared to the clever implementation in Ref. [3] which exploits the somewhat specific properties of the number 15. In Sec. III, we consider a Josephson charge-qubit model and derive the Hamiltonian describing the physical system. Additionally, we discuss how to control the quantum state of a register. Section IV presents the numerical methods which we have employed to find the physical implementations of the modules in the quantum-gate library. The evaluation of the time-development operator is straightforward once the externally controlled physical parameters are given. We solve the inverse problem; namely, we find the proper sequence for the control variables which produce the given quantum gate. Finally, in Sec. V, we combine the results obtained so far and present in detail how one would realize Shor's algorithm using Josephson charge qubits to factorize the number 15. We also discuss the robustness of the implementation. Section VI is devoted to a discussion of this realization.

II. SHOR'S FACTORIZATION ALGORITHM

The current extensive utilization of a variety of public-key cryptography methods and protocols based on the RSA algorithm [30] relies on the computational difficulty to factorize a large integer. The almost one-way nature of the modular exponential function serves to guarantee that although the encryption key, a large integer, is published the decryption of a message is a very difficult task. No classical algorithm for factoring a composite number N in polynomial time is known, although the potential existence of such an algorithm cannot be ruled out yet. In contrast, with the help of a quantum computer, the decryption of any RSA-based coding would be possible in polynomial time. As a curiosity, we note that the classical polynomial-time algorithm for the prime check of a given integer has recently been found [31].

The strategy for the factorization of a composite number $N = pq$, p and q being primes, using a quantum computer relies on finding the period r of the modular exponential function $f(x) = a^x \pmod{N}$, where $a < N$ is a random number coprime to N . For an even r , at least one prime factor of N is given by $\gcd(a^{r/2} \pm 1, N)$. In this

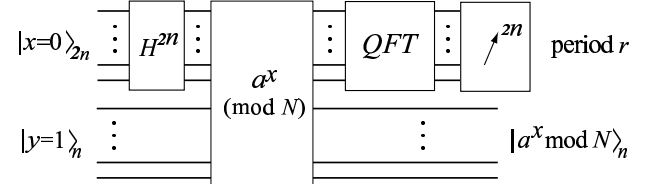


FIG. 1: Quantum circuit for Shor's algorithm.

paper we concentrate on the quantum circuit [43] needed for finding the period r , see Fig. 1. To obtain the implementation which involves minimal number of qubits, we follow a design which assumes that the fixed numbers a and N are hard-wired into the structure of the quantum circuit. However, if a large number of qubits is available, the design can be easily modified to take the numerical values of the numbers a and N residing in the separate quantum registers. The hard-wired approach combined with as much classical computing as possible is considerably more attractive from the experimental point of view.

Shor's algorithm has five stages: (1) Initialization of the quantum registers. The number N takes $n = \lceil \log_2(N+1) \rceil$ bits to store into memory, where $\lceil f \rceil$ stands for the nearest integer number equal to or greater than f . Thus we need two registers: $2n$ qubits for the register $|x\rangle_{2n}$ to store the number x and n qubits for the register $|y\rangle_n$ to store the value of the modular exponential function. The register $|x\rangle_{2n}$ is initialized as $|0\rangle_{2n}$ whereas $|y\rangle_n = |1\rangle_n$. (2) The elegance of a quantum computer — in contrast to a classical computer — arises from the possibility to utilize arbitrary superpositions. We generate the superposition state of all integers into the register $|x\rangle_{2n}$ by applying the Hadamard gate H to each qubit separately. (3) The execution of the algorithm, the time evolution $U(t)$, entangles each input value x with the corresponding value of the modular exponential function $f(x)$:

$$U \sum_x |x\rangle |1\rangle = \sum_x |x\rangle |a^x \pmod{N}\rangle. \quad (1)$$

The implementation of this part of the algorithm sets the limits for the spatial and temporal requirements of computational resources. (4) The quantum Fourier transformation (QFT) is applied to the register $|x\rangle_{2n}$, which squeezes the probability amplitudes into peaks due to the periodicity of the values of $f(x)$. (5) A measurement of the register $|x\rangle_{2n}$ finally gives an indication of the period r . The measurement is considered to be a projec-

tive nonunitary operation on the quantum register since it entangles the state of the quantum register into the macroscopic degrees of freedom of the measurement apparatus. A repetitive execution of the algorithm finally reveals the probability distribution which is peaked at the value $2^{2n}/r$ and its integer multiples in the output values at register $|x\rangle_{2n}$.

In addition to the quantum algorithm which is used to resolve the period r , a considerable amount of classical precomputing and postprocessing is needed as well. However, all this computing can be performed in polynomial time. Shor's algorithm is discussed in detail in many textbooks and research articles, such as Refs. [23, 30, 32, 33].

A. Decomposing the modular exponential function

The evaluation of the modular exponential function $f(x) = a^x \pmod{N}$ is the central part of Shor's algorithm. Thus we devote this section to finding the quantum circuit which performs this task.

A quantum algorithm is a unitary operator which evaluates the desired function $|f(x)\rangle$ starting from an initial state $|x\rangle$ in a reversible manner. The reversibility requirement for the function $f(x)$ can be circumvented by introducing additional scratch space into the quantum register. There exist various approaches to implementing the modular exponential function reversibly. The implementations differ in the number of gates and qubits needed and in the scaling behavior for large n . Clearly, to obtain an experimentally feasible implementation, the minimization of both of these numbers is important. On one hand, the decoherence time sets a limit to the length of the gate sequence while, on the other hand, many-qubit registers are hard to realize.

The remarkable experimental results [3] to factorize the number 15 involve an elegant quantum circuit of seven qubits and only a few simple quantum gates. However, this implementation definitely exploits the special properties of the number 15, and the fact that the outcome of the function $a^x \pmod{N}$ can be classically calculated in advance for all input values x when N is small.

We are, however, looking for a scalable reversible algorithm to implement any required modular exponential function. The classical well-known arithmetic algorithms are irreversible by nature but they can be implemented reversibly by replacing the standard logic gates by their reversible counterparts [37, 40]. To minimize the number of elementary-gate operations, we should utilize the classical Schönhage-Strassen [34] multiplication algorithm, which takes $O(n^2 \log_2 n \log_2 \log_2 n)$ time and $O(n \log_2 n \log_2 \log_2 n)$ space. Surely it will be the most appealing choice for very large integers N . For small N , the longhand multiplication algorithm provides the shortest gate array; furthermore, it only takes $O(n)$ space. For large n it scales sub-optimally, but still polynomially. An excellent review of classical arithmetic algorithms is presented in Ref. [34].

Our approach follows the implementation of the modular exponential function using a longhand multiplication algorithm and a QFT-based adder [35] which provides us with small scratch space requiring only a total space of $4n + 2$ qubits. The conventional approach to longhand multiplication without a QFT-based adder would require $O(5n)$ space. The price of the reduced space is the increase in the execution time, which now is $O(n^4)$, but which can be reduced down to $O(n^3 \log_2 \frac{n}{\epsilon})$, allowing for a certain error level ϵ . According to Ref. [35] one would achieve an algorithm requiring only $2n + 3$ qubits by introducing the intermediate measurement gates to the circuit. However, we do not utilize this realization since it is likely that the measurement at the intermediate step of the algorithm may easily introduce decoherence in the Josephson charge-qubit model.

When longhand multiplication is used, the implementation of the modular exponential function consists of three stages: (1) Writing out the modular exponential function as modular products (e.g., $a^2 = a \cdot a$), (2) Writing out the modular products as modular sums (e.g., $a \cdot a = \underbrace{a + \dots + a}_{a \text{ times}}$), (3) Finding the set of quantum gates that implements the modular sum.

First, we exploit a trick to compute the modular exponential function in terms of modular products:

$$a^x \equiv \prod_{i=0}^{2n-1} (a^{2^i x_i} \pmod{N}) \pmod{N}, \quad (2)$$

where we have used the binary expansion $x = 2^0 x_0 + 2^1 x_1 + 2^{n-1} x_{n-1}$, $x_i \in \{0,1\}$. Note that the number of terms in Eq. (2) grows only linearly for increasing n . Thus the modular exponential gate can be decomposed into a series of controlled modular multiplication gates (CMMUL(a^{2^i})), see Fig. 2. The values of $a^{2^i} \pmod{N}$ are fixed numbers and thus the implementation of the gate CMMUL(a^{2^i}) is fixed for each number a at the design stage. Here we use notation $C^k U$ or controlled ^{k} U to indicate that the gate operation U is performed only in the subspace where all the k control qubits are in the state $|1\rangle$.

Since a and N are coprimes and $a, x < N$ the gate CMMUL(a^{2^i}) is reversible; it only permutes the basis vectors. Depending on the cycle p of the permutation, $U_{\text{MMUL}(a^{2^i})}$ may represent an identity operation. Consequently, gates for which $xa^{2^j} \equiv 1 \pmod{N}$, $j > p$ can be drop out. For small numbers N , the cycle p is small compared to the number of gates. Thus considerable cancellation occurs. However, in the limit of large n , the cancellation is very rare. One should note that actually no quantum computer would be needed if the cycle p were found in the design phase.

The second stage of the decomposition is to find the sequence of modular adder gates (MADD) which corresponds to a given MMUL(a^{2^i}) gate. The longhand mul-

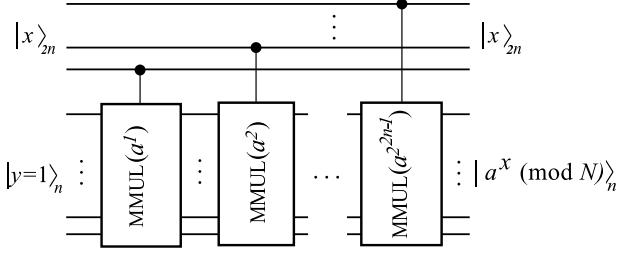


FIG. 2: Quantum circuit required for performing the evaluation of the modular exponential function utilizing the CMULL(b) gates.

multiplication obeys the relation

$$a^{2^i} x \equiv \sum_{i=0}^{2n-1} (a^{2^i} 2^i x_i \pmod{N}) \pmod{N}, \quad (3)$$

which again involves only a linear number of terms.

The resulting quantum circuit performing the CMMUL(a^{2^i}) gate is depicted in Fig. 3; each multiplier gate is decomposed into a sequence of CMADD(b) gates, where b is a dummy variable. Since this decomposition of CMMUL(a^{2^i}) requires extra space for the intermediate results, we are forced to introduce a scratch space $|z\rangle_n$ into the setup. Initially, we set $|z\rangle_n = |0\rangle_n$. Moreover, we must reset the extra scratch space after each multiplication. This is accomplished by multiplication with the inverse element b^{-1} . Let us consider how the gate CMMUL(b) works:

$$\begin{aligned} |x\rangle|0\rangle &\rightarrow |x\rangle|0 + bx \pmod{N}\rangle && \text{(product)} \\ &\rightarrow |bx \pmod{N}\rangle|x\rangle && \text{(swap)} \\ &\rightarrow |bx \pmod{N}\rangle|x + (-b^{-1})(bx \pmod{N})\rangle \\ &= |bx \pmod{N}\rangle|0\rangle. && \text{(result)} \end{aligned}$$

Euler's totient theorem guarantees that for every b which is coprime to N , a modular inverse $b^{-1} \in \mathbb{N}$ exists. Furthermore, the extended Euclidean algorithm provides an efficient way to find the numerical value for b^{-1} .

Now we are left with the final task: how to implement the controlled² modular adder. There exists several propositions in the literature, see Refs. [35, 37]. We adopt the elegant approach by Beauregard which allows the addition to be performed in the Fourier space, see Fig. 4. For this realization we need only to add one extra qubit to register $|z\rangle_n$ and to introduce one ancilla qubit $|a\rangle$. An obvious drawback of this implementation is the need for a number of QFT-gates. Figure 5 represents the familiar decomposition [38] of a QFT-gate into one- and two-qubit gates. Formally, the number of elementary gates for a QFT scales as $O(n^2)$. However, allowing for a certain finite error level ϵ and discarding the smallest phase shifts we can have $O(n \log_2 \frac{n}{\epsilon})$ for large n .

The decomposition of the gate C²MADD(b) consists of controlled² adders, $(n + 1)$ -qubit QFTs, one-qubit NOTs, and CNOTs. Since the Fourier space is utilized, the C²ADD(b) gates can be implemented [36] using controlled² phase shifts, see Fig. 6. The quantum gate

sequence for an adder working in the Fourier space is depicted in Fig. 6. The values of the phase shifts for the gate C²ADD(b) are given by $e^{2\pi i \phi_j / 2^n}$, where $\phi_j = 2^j b$.

Finally we are in the position to perform the unitary transformation which implements the modular exponential function using only one-, two- and three-qubit modules. If the three-qubit gates are not available, further decomposition into one- and two-qubit gates is needed, see Ref. [17]. For instance, each three-qubit controlled²U gate decomposes into five two-qubit gates and each Fredkin gate takes seven two-qubit gates to implement.

Minimizing the number of gates is important not only for shortening the execution time but also for decreasing the error. If the physically implemented gate operations U_i are imperfect, the output of the quantum circuit differs from the desired one. Let us assume that $U_i = \hat{U}_i + \epsilon_i$, where \hat{U}_i are the desired gate operations and ϵ_i stand for small errors. The total error E for an l -gate circuit can be approximated by

$$E = \|U - \hat{U}\| \leq l \times \epsilon_{\max}. \quad (4)$$

In order to accomplish an l -gate quantum circuit with a reasonable error level, one must implement every gate operation with an accuracy of $\|\epsilon_i\| < 1/l$. The ability to implement the same algorithm using a shorter gate sequence will be likely to yield more accurate results.

B. Three-qubit modules

A quantum gate V_k acting on the first k qubits in the quantum register stands for a unitary operator in the space \mathbb{C}^{2^n}

$$U = e^{\phi i} V_k \bigotimes_{n-k} I_{2 \times 2}, \quad (5)$$

where the identity operator acts on the dimensions of the inactive qubits. It is always possible to choose $V_k \in SU(2^k)$ since the difference between a unitary and the related special unitary matrix can be compensated for by a global phase difference ϕ which is physically meaningless. The gate which acts on other than the first k qubits is obtained by permuting the basis vectors $U' = \Pi U \Pi^{-1}$. If only nearest neighbor interactions are available, the permutation matrix Π must be implemented using e.g. SWAP gates. However, in the physical model that we consider in Sec. III the permutations are merely a notational difficulty. Thus, we may directly design n -qubit modules between any n qubits.

Figure 7 illustrates the set of modules that we utilize for the implementation of Shor's algorithm. As explained above, $V_k \in SU(2^k)$. Hence we can represent any quantum gate V_k by a $2^k \times 2^k$ unimodular complex matrix. In our notation the basis vectors are labeled according to the usual convention e.g., $|00\rangle = (1000)^T$, $|01\rangle = (0100)^T$.

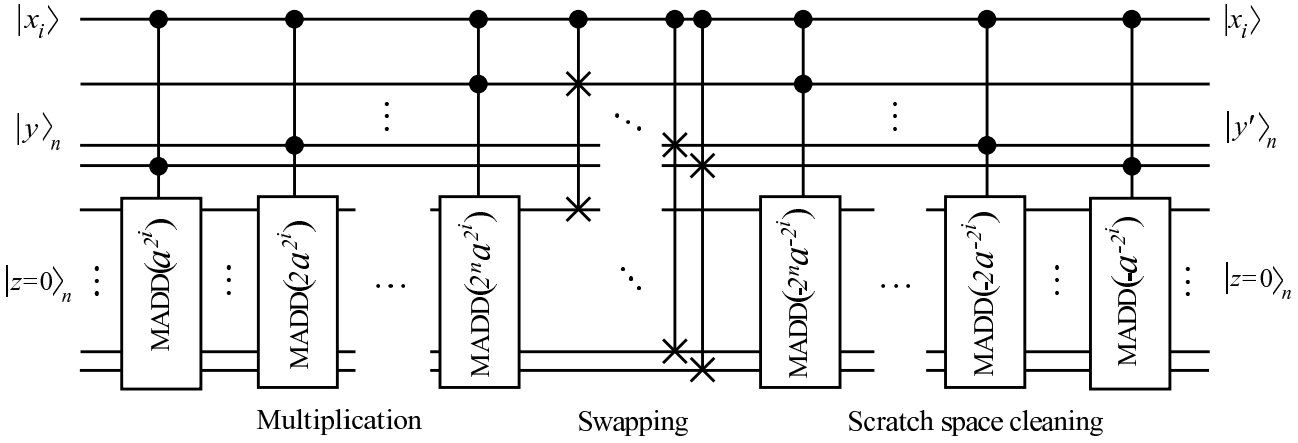


FIG. 3: Decomposition of $\text{CMMULL}(a^{2^i})$ gate using $\text{C}^2\text{MADD}(b)$ and controlled swap gates. If the controlling qubit $|x_i\rangle$ is active the resulting state is $y' \equiv y + a^{2^i} \pmod{N}$, otherwise $y' = y$. Note, that the gate utilizes an additional ancilla register $|z\rangle_n$ to perform the calculation.

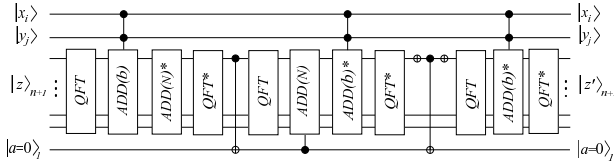


FIG. 4: Decomposition of the $\text{C}^2\text{MADD}(b)$ gate into elementary gates, QFT gates, and additions in the Fourier basis (C^2ADD). The asterisk stands for a Hermitian conjugate; it corresponds to a gate for subtraction. The gate takes input value $z < N \leq 2^n$ and yields $|z'\rangle = |z + b \pmod{N}\rangle$ if the control qubits $x_i = 1$ and $y_j = 1$. Otherwise $|z'\rangle = |z\rangle$. The gate utilizes one ancilla qubit $|a\rangle$ to indicate whether the intermediate result $z + b > N$. In fact, the highest qubit in the $|z\rangle$ register is also an ancilla since it is zero before and after the gate operation.

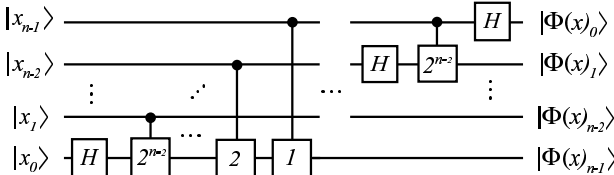


FIG. 5: Quantum circuit for an n -qubit Fourier transformation. Here H stands for the Hadamard gate. The controlled phase-shift gates are labeled with the numbers k which correspond to the phase shifts $e^{i2\pi k/2^n}$. Note the reversed order of the qubits on the right-hand side.

We now give an explicit matrix representation for the required low-order gates. The Hadamard gate is

$$U = \frac{e^{i\pi/2}}{\sqrt{2}} \begin{bmatrix} 1 & 1 \\ 1 & -1 \end{bmatrix}. \quad (6)$$

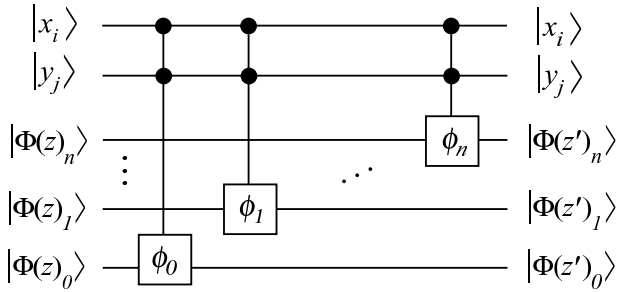


FIG. 6: Quantum circuit for the controlled² addition of a classical number b into the quantum register $|z\rangle$ in the Fourier basis. The controlled² phase-shift gates serve to yield the phase shift $e^{2\pi i \phi_k/2^n}$ provided that the control qubits $|x_i\rangle$ and $|y_j\rangle$ are active.

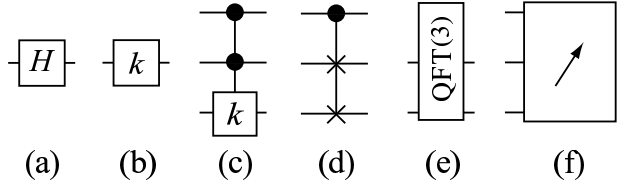


FIG. 7: Low-order modules for Shor's algorithm. From left to right: (a) Hadamard, (b) phase-shift, (c) controlled² phase-shift, (d) Fredkin (controlled SWAP), (e) quantum Fourier transformation, and (f) the measurement gate.

The CNOT gate equals

$$U = e^{i\pi/4} \begin{bmatrix} 1 & 0 & 0 & 0 \\ 0 & 1 & 0 & 0 \\ 0 & 0 & 0 & 1 \\ 0 & 0 & 1 & 0 \end{bmatrix}. \quad (7)$$

The two-qubit SWAP gate is represented by

$$U = e^{i\pi/4} \begin{bmatrix} 1 & 0 & 0 & 0 \\ 0 & 0 & 1 & 0 \\ 0 & 1 & 0 & 0 \\ 0 & 0 & 0 & 1 \end{bmatrix}. \quad (8)$$

The Fredkin (controlled SWAP) gate is

$$U = e^{i\pi/8} \begin{bmatrix} 1 & 0 & 0 & 0 & 0 & 0 & 0 & 0 \\ 0 & 1 & 0 & 0 & 0 & 0 & 0 & 0 \\ 0 & 0 & 1 & 0 & 0 & 0 & 0 & 0 \\ 0 & 0 & 0 & 1 & 0 & 0 & 0 & 0 \\ 0 & 0 & 0 & 0 & 1 & 0 & 0 & 0 \\ 0 & 0 & 0 & 0 & 0 & 1 & 0 & 0 \\ 0 & 0 & 0 & 0 & 0 & 0 & 1 & 0 \\ 0 & 0 & 0 & 0 & 0 & 0 & 0 & 1 \end{bmatrix}. \quad (9)$$

The matrix presentation for the phase-shift gate is

$$U = e^{-i2\pi k/2^{n+1}} \begin{bmatrix} 1 & 0 \\ 0 & a_k \end{bmatrix}, \quad (10)$$

where $a_k = e^{i2\pi k/2^n}$, with n denoting the number of qubits that the gate operates on. We have chosen this phase convention since all the phase shifts needed can be expressed with a positive integer k , instead of a fractional number. Low k values correspond to small phase shifts.

The controlled phase-shift gate is

$$U = e^{-i2\pi k/2^{n+2}} \begin{bmatrix} 1 & 0 & 0 & 0 \\ 0 & 1 & 0 & 0 \\ 0 & 0 & 1 & 0 \\ 0 & 0 & 0 & a_k \end{bmatrix}. \quad (11)$$

Similarly, the controlled² phase-shift gate is

$$U = e^{-i2\pi k/2^{n+3}} \begin{bmatrix} 1 & 0 & 0 & 0 & 0 & 0 & 0 & 0 \\ 0 & 1 & 0 & 0 & 0 & 0 & 0 & 0 \\ 0 & 0 & 1 & 0 & 0 & 0 & 0 & 0 \\ 0 & 0 & 0 & 1 & 0 & 0 & 0 & 0 \\ 0 & 0 & 0 & 0 & 1 & 0 & 0 & 0 \\ 0 & 0 & 0 & 0 & 0 & 1 & 0 & 0 \\ 0 & 0 & 0 & 0 & 0 & 0 & 1 & 0 \\ 0 & 0 & 0 & 0 & 0 & 0 & 0 & a_k \end{bmatrix}. \quad (12)$$

A quantum Fourier transformation (QFT) is defined for any number k of qubits by the generic matrix element

$$(U_k)_{n,m} = e^{s2\pi i/2^{k+1}} \frac{1}{\sqrt{2^k}} e^{2\pi i n m / 2^k}, \quad (13)$$

where $s = 1$ for a two-qubit QFT, otherwise $s = -1$.

III. JOSEPHSON CHARGE-QUBIT REGISTER

In this Section we derive the Hamiltonian for an ideal Josephson charge-qubit register. We also comment on the experimentally accessible parameter regions. The present

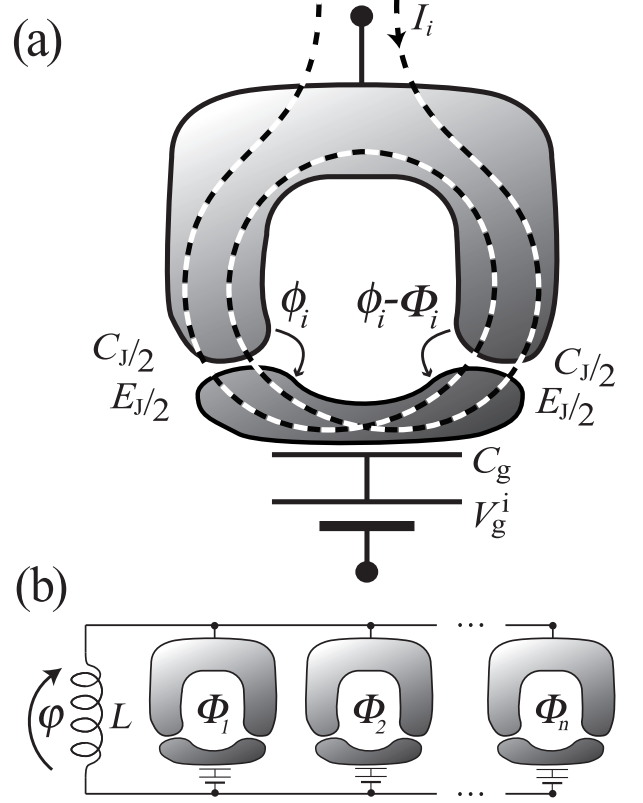


FIG. 8: a) Schematic of a Josephson charge qubit with the relevant parameters. b) An array of Josephson charge qubits coupled in parallel with an inductor.

setting, as well as other related realizations of quantum computing, have been analyzed in the Ref. [16]. It is, however, instructive to consider the derivation in detail here since it will reveal some subtleties. We note, in particular, that our quantum-gate construction scenario in Sec. IV relies on a piecewise linear rather than a piecewise constant time dependence of the control parameters. We will also try to list the limitations of the model.

A. The Lagrangian

Consider a homogenous array of mesoscopic superconducting islands as an idealized model of a quantum register, see Fig. 8. The basis states of the qubit correspond to either zero or one extra Cooper pair residing on the superconducting island, denoted by $|0\rangle$ and $|1\rangle$, respectively. Each of the islands, or Cooper-pair boxes, is capacitively coupled to a gate voltage, V_g^i . In addition, they are coupled to a superconducting lead through a mesoscopic SQUID with identical junctions, each having the same Josephson energy $E_J/2$ and capacitance $C_J/2$. All these qubits are then coupled in parallel with an inductor, L . The lowest relevant energy scale is set by the thermal energy $k_B T$ and the highest scale by the BCS gap Δ_{BCS} .

We assume that the gate voltage V_g^i and the time-dependent flux Φ_i through each SQUID can be controlled externally. The flux Φ_i may be controlled with an adjustable current I_i through an external coil, see the dotted line in Fig. 8a. In this setup, the Cooper pairs can tunnel coherently to a superconducting electrode. We denote the so-called flux difference (i.e. the time-integral of voltage) over, say, the left junction of the i^{th} SQUID by ϕ_i and the flux difference over the inductor by φ . Consequently, the flux difference over the rightmost junction is $\phi_i - \Phi_i$. We take the positive direction for flux to be directed outward normal to the page.

We adopt ϕ_i and φ as the dynamical variables, whereas Φ_i and V_g^i are external adjustable parameters. With the help of elementary circuit analysis [39], we obtain the Lagrangian for the qubit register

$$\mathcal{L} = \frac{1}{2} \sum_{i=1}^n \left[\frac{C_J}{2} \dot{\phi}_i^2 + \frac{C_J}{2} (\dot{\phi}_i - \dot{\Phi}_i)^2 + C_g (\dot{\phi}_i + \varphi - V_g^i)^2 \right] - \frac{\varphi^2}{2L} + \frac{1}{2} \sum_{i=1}^n \left[E_J \cos \left(\frac{2e}{\hbar} \phi_i \right) + E_J \cos \left(\frac{2e}{\hbar} (\phi_i - \Phi_i) \right) \right]. \quad (14)$$

We now perform the following changes of variables

$$\phi_i \rightarrow \phi_i + \frac{\Phi_i}{2} - \frac{C_g}{C_J + C_g} \varphi. \quad (15)$$

This will serve two purposes. It will diagonalize the Lagrangian (as well as the corresponding Hamiltonian) and it will also allow us to rewrite the potential energy contribution in Eq. (14) in a more transparent form. It is convenient to carry out these transformations before proceeding to the Hamiltonian formalism since in this way we need not consider any commutation relations or modifications to the derivative terms due to the interaction picture. The change of variables yields

$$\begin{aligned} \mathcal{L} = & \frac{1}{2} \sum_{i=1}^n \left[(C_J + C_g) \dot{\phi}_i^2 - 2C_g \left(V_g^i - \frac{\dot{\Phi}_i}{2} \right) \dot{\phi}_i \right. \\ & \left. + E_J \cos \left(\pi \frac{\Phi_i}{\Phi_0} \right) \cos \left(\frac{2e}{\hbar} \phi_i - \frac{2\pi C_{\text{qb}}}{\Phi_0 C_J} \varphi \right) \right] \\ & + \frac{1}{2} NC_{\text{qb}} \dot{\varphi}^2 - \sum_{i=1}^n C_{\text{qb}} \left(V_g^i - \frac{\dot{\Phi}_i}{2} \right) \dot{\varphi} - \frac{\varphi^2}{2L} \quad (16) \end{aligned}$$

$$+ \text{const.} \quad (17)$$

Above, $\Phi_0 = \frac{\hbar}{2e}$ is the flux quantum and

$$C_{\text{qb}} = \frac{C_J C_g}{C_J + C_g} \quad (18)$$

is the qubit capacitance in the LC -circuit. Note that the effective Josephson energy of each SQUID can now be tuned. We denote this tunable energy parameter in Eq. (17) as

$$E_J(\Phi_i) = E_J \cos \left(\pi \frac{\Phi_i}{\Phi_0} \right). \quad (19)$$

The canonical momenta are given by

$$Q = \frac{\partial \mathcal{L}}{\partial \dot{\varphi}} \quad (20)$$

and

$$q_i = \frac{\partial \mathcal{L}}{\partial \dot{\phi}_i}. \quad (21)$$

We interpret Q as the charge on the collective capacitor formed by the whole qubit register, whereas q_i is the charge on the i^{th} island. Note that the charge q_i is related to the number n_i of Cooper pairs on the island through $q_i = -2en_i$.

B. The Hamiltonian

We are now in the position to write down the Hamiltonian for the quantum register. We will also immediately replace the canonical variables by operators in order to quantize the register. Moreover, we will employ the number of Cooper pairs n_i on the island and the superconducting phase difference instead of the usual quantum-mechanical conjugates. We will also change to the more common phase difference θ_i related to ϕ_i through $\theta_i = \frac{2e}{\hbar} \phi_i$. The relevant commutation relations are hence

$$[\theta_i, n_i] = -i \quad (22)$$

and

$$[\varphi, Q] = i\hbar. \quad (23)$$

All the other commutators vanish

$$[\theta_i, \varphi] = [n_i, Q] = [\theta_i, Q] = [n_i, \varphi] = 0. \quad (24)$$

Using the Legendre transformation

$$\mathcal{H} = Q \dot{\varphi} + \sum_{i=1}^n q_i \dot{\phi}_i - \mathcal{L} \quad (25)$$

we obtain

$$\begin{aligned} \mathcal{H} = & \sum_{i=1}^n \left[\frac{2e^2 (n_i - n_g^i)^2}{C_J + C_g} - E_J(\Phi_i) \cos \left(\theta_i - \frac{2\pi C_{\text{qb}}}{\Phi_0 C_J} \varphi \right) \right] \\ & + \frac{(Q + Q_g)^2}{2NC_{\text{qb}}} + \frac{\varphi^2}{2L}. \quad (26) \end{aligned}$$

We have denoted the effective gate charge by

$$n_g^i = \frac{C_g}{2e} \left(V_g^i - \frac{\dot{\Phi}_i}{2} \right) \quad (27)$$

and

$$Q_g = \sum_{i=1}^n C_{\text{qp}} \left(V_g^i - \frac{\dot{\Phi}_i}{2} \right). \quad (28)$$

It is important to note that in addition to the usual voltage contribution, the time dependence of the flux also plays a role. In practice, the rates of change of the flux are negligible in comparison to the voltages and this term may safely be dropped. In contrast, however, very sudden and strong pulses of flux may induce strong transient phenomena which complicate the qubit control. Nevertheless, the emf can be compensated with the voltage gate if necessary.

The Hamiltonian in Eq. (26) describes the register of quantum bits (n_i, ϕ_i) coupled to a quantum-mechanical LC -resonator, i.e., a harmonic oscillator (Q, φ) . We will now assume that the rms fluctuation of φ is small compared to the flux quantum Φ_0 and also that the harmonic oscillator has a sufficiently high frequency, such that it will stay in its ground state. The first assumption implies that

$$\cos\left(\theta_i - \frac{2\pi C_{\text{qb}}}{\Phi_0 C_{\text{J}}} \varphi\right) \approx \cos\theta_i + \frac{2\pi C_{\text{qb}}}{\Phi_0 C_{\text{J}}} \varphi \sin\theta_i . \quad (29)$$

The second assumption will cause an effective coupling between the qubits. Namely, the Hamiltonian may now be rewritten in the more suggestive form

$$\begin{aligned} \mathcal{H} \approx \sum_{i=1}^n & \left[\frac{2e^2(n_i - n_g^i)^2}{C_{\text{J}} + C_{\text{g}}} - E_{\text{J}}(\Phi_i) \cos\theta_i \right] \\ & + \frac{(Q + Q_g)^2}{2NC_{\text{qb}}} + \frac{(\varphi - \hat{\varphi})^2}{2L} - \frac{\hat{\varphi}^2}{2L}, \end{aligned} \quad (30)$$

where the operator $\hat{\varphi}$ is given by

$$\hat{\varphi} = \frac{2\pi LC_{\text{qb}}}{\Phi_0 C_{\text{J}}} \sum_{i=1}^n E_{\text{J}}(\Phi_i) \sin\theta_i . \quad (31)$$

We now see from Eq. (30) that in the high-frequency limit the harmonic oscillator is effectively decoupled from the qubit register. The effect of the qubit register is thus to redefine the minimum of the potential energy for the oscillator. This does not affect the spectrum of the oscillator, since it will adiabatically follow its ground state in the low-temperature limit. We may therefore trace over the degrees of freedom of the harmonic oscillator and the harmonic-oscillator energy will merely yield a zero-point energy contribution, $\hbar\omega_{LC}/2$. The effective Hamiltonian describing the dynamics of the coupled qubit register alone is thus

$$\begin{aligned} \mathcal{H} \approx \sum_{i=1}^n & \left[\frac{2e^2(n_i - n_g^i)^2}{C_{\text{J}} + C_{\text{g}}} - E_{\text{J}}(\Phi_i) \cos\theta_i \right] \\ & - \frac{2\pi^2 LC_{\text{qb}}^2}{\Phi_0^2 C_{\text{J}}^2} \left(\sum_{i=1}^n E_{\text{J}}(\Phi_i) \sin\theta_i \right)^2 . \end{aligned} \quad (32)$$

This result is in agreement with the one presented in Ref. [16]. We may conclude that the LC -oscillator has created a virtual coupling between the qubits.

For the purposes of quantum computing, it is convenient to truncate the Hilbert space such that each Cooper-pair box will have only two basis states. In the limit of a high charging energy $E_{\text{C}} = 2e^2/(C_{\text{g}} + C_{\text{J}})$ relative to the Josephson energy E_{J} , we may argue that in the region $0 \leq n_g^i \leq 1$ only the states with $n_i = 0, 1$ can be occupied. We use the vector representation for these states, in which

$$|0\rangle_i = \begin{pmatrix} 1 \\ 0 \end{pmatrix}_i \quad (33)$$

and

$$|1\rangle_i = \begin{pmatrix} 0 \\ 1 \end{pmatrix}_i . \quad (34)$$

The basis states of the Hilbert space are orthogonal $\langle n | e^{\pm i\theta} | m \rangle = \delta_{n,m} \mp 1$. Hence, in this two-state approximation, $\cos\theta_i = \frac{1}{2}\sigma_x^i$ and $\sin\theta_i = \frac{1}{2}\sigma_y^i$, where, e.g., σ_x^i stands for $I \otimes \dots \otimes \sigma_x \otimes I \dots \otimes I$. Finally, omitting the constant terms, we obtain the Hamiltonian in the Pauli-matrix representation

$$\begin{aligned} \mathcal{H}_{\text{qp}} = \sum_{i=1}^n & \left[-\frac{E_{\text{C}}}{2}(1 - 2n_g^i)\sigma_z^i - \frac{E_{\text{J}}(\Phi_i)}{2}\sigma_x^i \right] \\ & - \frac{\pi^2 L}{\Phi_0^2} \left(\frac{C_{\text{qb}}}{C_{\text{J}}} \right)^2 \sum_{i=1}^n \sum_{j=i+1}^n E_{\text{J}}(\Phi_i) E_{\text{J}}(\Phi_j) \sigma_y^i \otimes \sigma_y^j . \end{aligned} \quad (35)$$

The above Hamiltonian is a convenient model for studying the construction of quantum algorithms for a number of reasons. First of all, each single-qubit Hamiltonian can in principle be set to zero, thereby eliminating all temporal evolution. Secondly, setting the effective Josephson coupling to zero may eliminate the coupling between any two qubits. This may be achieved by applying half a flux quantum through the SQUID loops. However, it is impossible to carry out one-qubit operations on several qubits simultaneously since the interqubit couplings do not vanish. If the Josephson energy of any two qubits is nonzero, there will automatically be a coupling between them. This is partly why numerical methods are convenient for finding control-parameter sequences. By properly tuning the gate voltages and fluxes it is possible to compensate undesired couplings and to perform any temporal evolution in this model setup.

We will from now on denote the i^{th} qubit Hamiltonian by

$$\mathcal{H}_{\text{single}}^i = -\frac{1}{2}B_z^i\sigma_z^i - \frac{1}{2}B_x^i\sigma_x^i \quad (36)$$

and the coupling between the i^{th} and j^{th} qubits by

$$\mathcal{H}_{\text{coupling}} = -CB_x^i B_x^j \sigma_y^i \otimes \sigma_y^j . \quad (37)$$

Above, $B_x^i = E_{\text{J}}(\Phi_i)$, $B_z^i = E_{\text{C}}(1 - 2n_g^i)$ and $C = \frac{\pi^2 L}{\Phi_0^2} \left(\frac{C_{\text{qb}}}{C_{\text{J}}} \right)^2$. The approach taken is to deal with the parameters B_z^i and B_x^i as dimensionless control parameters. We set $C = 1$ and choose natural units $\hbar = 1$.

We note that the generators σ_x and σ_z are sufficient to construct all the $SU(2)$ matrices through the Baker-Campbell-Hausdorff formula and thus single-qubit gates need not be constructed numerically. It is worth mentioning for practical reasons that we cannot achieve $U(2^n)$ for n qubits since the Hamiltonian for the entire quantum register turns out to be traceless. However, the global phase factor is not physical here since it corresponds to a redefinition of the zero level of energy.

C. Limitations of the model

Above we have outlined a derivation for the Hamiltonian which does not take any decoherence mechanisms into account. To justify this omission, we have to ensure that a charge-qubit register, or any other related scenario [8, 9, 11, 12, 13, 14] is decoherence-free for time scales long enough to execute a practical quantum algorithm. In addition, we have neglected the inhomogeneity of the SQUIDs. It may be extremely awkward to fabricate sufficiently uniform junctions. A three-junction design might alleviate this problem. Whereas for the control of N two-junction SQUIDs one needs at least N independent sources of flux, the three-junction design would call for $2N$ independent sources. The extra sources may be used to compensate the structural discrepancies. The noise in the control parameters has also been neglected but it will turn out that the error will grow linearly with the rms displacement of uncorrelated Gaussian noise. Correlated noise may only be tolerated if it is very weak. We have also neglected the issue of quantum measurement altogether in the above.

A crucial assumption is that $k_B T \ll E_J \ll E_C \ll \Delta_{BCS}$. Typical operation frequencies would be in the GHz range and the operation temperature could be tens of mK. For our two-state Hamiltonian to apply, we should actually insist that, instead of $E_J \ll E_C$, the requirement

$$E_J(\Phi_i) \ll E_C \quad (38)$$

holds. It may appear at first that B_x^i cannot take on values exceeding B_z^i . However, this does not hold since the gate charge also plays a role; values of B_z^i can be very small if n_g^i is tuned close to one half. Since we employ natural units we may freely rescale the Hamiltonian while rescaling time. This justifies our choice $C = 1$ above. Furthermore, it is always possible to confine the parameter values within an experimentally accessible range. For more discussion, see Ref. [16].

IV. IMPLEMENTING A QUANTUM-GATE LIBRARY

The physical implementation of a practical quantum algorithm requires that it is decomposed into modules whose physical realizations are explicitly known. Here we

consider methods to find the physical implementations for the modules for the quantum-gate library which is required for Shor's algorithm.

A. Unitary time evolution

The temporal evolution of the Josephson charge-qubit register is described by a unitary operator

$$U_{\gamma(t)} = \mathcal{T} \exp \left(-i \int_{\gamma(t)} H(\gamma(t)) dt \right), \quad (39)$$

where \mathcal{T} stands for the time-ordering operator and $H(\gamma(t))$ is the Hamiltonian of the qubit register. The integration is performed along the path $\gamma(t)$ which describes the time evolution of the control parameters in the space spanned by $\{B_x^j(t)\}$ and $\{B_z^j(t)\}$.

The parameter path $\gamma(t)$ with infinitely many degrees of freedom will be discretized using a finite set of parameters $X_{\gamma(t)}$. This is accomplished by restricting the path $\gamma(t)$ to a special class of loops, namely polygons in the parameter space. One could choose other types of discretizations as well. For instance, some set of smooth orthogonal functions may be experimentally attractive. For an n -qubit register, the control-parameter path $\gamma(t)$ is of the vector form

$$\gamma(t) = [B_z^1(t), \dots, B_z^n(t); B_x^1(t), \dots, B_x^n(t)]^T, \quad (40)$$

where $B_z^i(t)$ and $B_x^i(t)$ are piecewise linear functions of time in our discretization. Hence, in order to evaluate Eq. (39), one only needs to specify the $2n$ coordinates for the ν vertices of the polygon, which we denote collectively as X_{γ} . We let the parameter loop start at the origin, i.e., at the degeneracy point where no time development takes place. We further set the time spent in traversing each edge of the polygon to be unity. One could also take the speed at which each edge is traversed to be an additional free parameter, which would further accelerate the algorithm.

In our scheme, the execution time for each quantum gate depends linearly on the number ν of the vertices in the parameter path. This yields a nontrivial relation between the execution time of the algorithm and the size of the modules. First note that each k -qubit module represents a matrix in $SU(2^k)$. To implement the module, one needs to have enough vertices to parameterize the unitary group $SU(2^k)$, which has $2^{2k} - 1$ generators. In our model, we have $2k$ parameters for each vertex, which implies

$$2k\nu \geq 2^{2k} - 1. \quad (41)$$

We have used $\nu = 4$ for the two-, and $\nu = 12$ for the three-qubit modules. For yet larger modules, the length of the required parameter sequence grows rapidly. In general, we expect that the quantum algorithm is accelerated by the availability of larger modules. However,

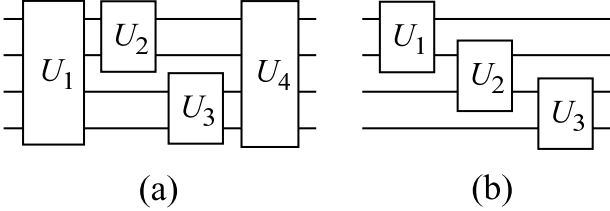


FIG. 9: Comparison of the quantum circuits with different optimal sizes of modules. (a) One general four-qubit module U' absorbs all the gates U_i and accelerates the algorithm considerably. (b) The two-qubit gates U_i require in total shorter parameter sequences than the general four-qubit module U' .

the optimal size of the modules is highly nontrivial and requires further considerations, see Fig. 9.

To evaluate the unitary operator $U_{\gamma(t)}$ we must find a numerical method which is efficient, yet numerically stable. We divide the path $\gamma(t)$ into tiny intervals that take the time Δt to traverse. If γ_i denotes all the values of the parameters in the midpoint of the i^{th} interval, and m is the number of such intervals, then we find to a good approximation

$$U_{X_\gamma} \approx \exp(-iH(\gamma_m)\Delta t) \dots \exp(-iH(\gamma_1)\Delta t). \quad (42)$$

To accurately evaluate the matrix exponentials, we employ the spectral decomposition

$$e^A = \sum_k e^{\lambda_k} |\lambda_k\rangle\langle\lambda_k|, \quad (43)$$

where λ_k and $|\lambda_k\rangle$ stand for the eigenvalues and the corresponding eigenvectors of the matrix A . However, the evaluation of the eigenvectors and the eigenvalues requires much computation. A more efficient method is to utilize the truncated Taylor series

$$e^A \approx \sum_{k=0}^l \frac{A^k}{k!}, \quad (44)$$

where l is a small integer. We use the Taylor-series expansion to evaluate the matrix $U_{\gamma(t)}$ for various paths $\gamma(t)$ and confirm the approximation by using the spectral decomposition.

B. Minimization of the error function

Given an arbitrary gate operation \hat{U} , our aim is to find a parameter sequence X_γ for the Josephson charge-qubit register that would yield a unitary matrix U_{X_γ} which equals \hat{U} . We convert the inverse problem into an optimization task; namely, finding the zeroes of the error function

$$f(X_\gamma) = \|\hat{U} - U_{X_\gamma}\|_F. \quad (45)$$

Minimizing the error function $f(X_\gamma)$ over all the possible values of X_γ will produce an approximation U_{X_γ} for

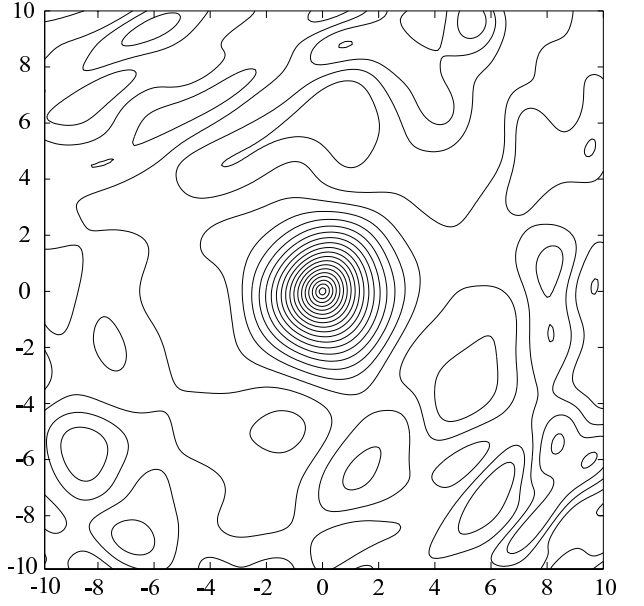


FIG. 10: Typical planar cut of the 72-dimensional error function space. The plane through the minimum point X_{\min} has been chosen arbitrarily in the parameter space.

the desired gate \hat{U} . Above $\|\cdot\|_F$ is the Frobenius trace norm, defined as $\|A\|_F = \sqrt{\text{Tr}(A^\dagger A)}$, which is numerically efficient to compute. Since all the matrix norms are mathematically equivalent, a small value of $\|A\|_F$ implies a small value in all other norms; specifically, there exist positive constants c and C , independent of A , for which $c\|A\|_2 \leq \|A\|_F \leq C\|A\|_2$.

For this minimization problem, the error-function landscape is rough consisting of many local minima, see Fig. 10. Consequently, any gradient-based minimization algorithm will encounter serious problems. We have found the minimum point X_{\min} for all the gates presented in Sec. V using repeated application of a robust polytope algorithm [41, 42]. In the first search, the initial condition was chosen randomly. At the next stage, the outcome of the previous search was utilized. In order to accelerate the evaluation of $U_{\gamma(t)}$ we varied the time steps Δt ; at an early stage of the optimization a coarse step was employed while the final results were produced using very fine steps. Typical convergence of the search algorithm is illustrated in Fig. 11.

The required accuracy for the gate operations is in the range $10^{-4} - 10^{-5}$ in the error-function values for two reasons: (i) in quantum circuits with a small number of gates, the total error remains small, see Eq. (4), and (ii) for large circuits, quantum-error correction can in principle be utilized to reduce the accumulated errors [28]. Our minimization routine takes on the order of 10^6 function evaluations to reach the required accuracy. Each of the error-function evaluations takes about 0.1 seconds on a PC. Thus, it is clear that parallel processing is needed to solve the problem in reasonable wall-clock time. Fortunately, the particular optimization tasks consist of inde-

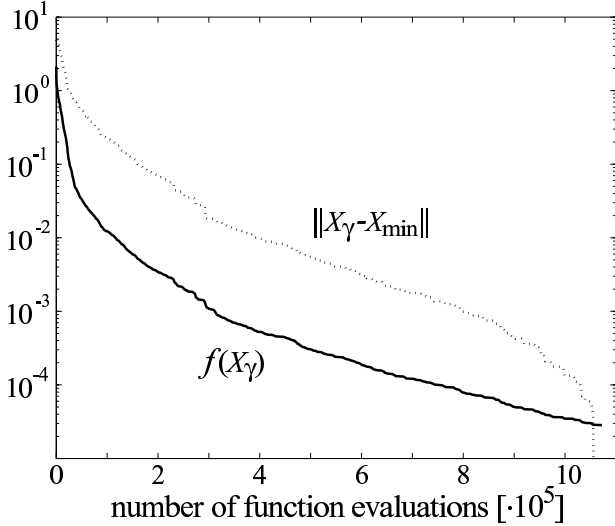


FIG. 11: Convergence of the algorithm for the Fredkin gate. The error function values are indicated by the solid line and the distance of the parameter sequence from the numerical optimum X_{\min} by dotted line.

pendent matrix multiplications which can be evaluated simultaneously.

To parallelize the calculation using N processors, we divide the polygonal path $\gamma(t)$ into N intervals which all consist of the same number of matrix products to evaluate. The parameters of the intervals are sent to separate processors in the parallel-processing system, which perform the laborious calculation. The resulting unitary matrices are collected and their product is evaluated. Neither fast interconnections between the processors nor large memories are required.

V. EXAMPLE

To demonstrate the level of complexity of the quantum circuit and the demands for the execution time, here we explicitly represent the quantum circuit and some physical implementation for the gates needed for Shor's algorithm to factorize the number $N = 15$. The algorithm requires no *a priori* knowledge about the properties of the number 15.

A. Quantum Circuit

We consider the decomposition of Shor's algorithm explained in Sec. II. First we note that $\log_2 16 = 4$. Thus, the register $|y\rangle$ must consist of 4 qubits and the register $|x\rangle$ should consist of 8 qubits. For scratch space we need a five-qubit register $|z\rangle_5$ and one ancilla qubit $|a\rangle$.

When decomposing the modular exponential function we encounter a special situation: $7^4 \equiv 1 \pmod{15}$, which implies that we actually know at this stage

that the period of the modular exponential function is 4. To illustrate the structure of the algorithm, we continue its construction and just note that only two, instead of eight, qubits are needed for the register $|x\rangle$. Consequently, the decomposition of the modular exponential function consists of two controlled multiplication gates: CMMUL(7) and CMMUL(7^2). In the general situation, we would also need the gates CMMUL(7^4), CMMUL(7^8), CMMUL(7^{16}), CMMUL(7^{32}), CMMUL(7^{64}), and CMMUL(7^{128}), but we omit them for simplicity.

The longhand multiplication decomposes each controlled multiplication into four controlled² adders. Since the adders work in the Fourier space $\text{QFT}(5)/\text{QFT}^*(5)$ gates are needed before and after each adder sequence. First, to implement the CMMUL(7) gate, we need the following controlled² adder gates: C²MADD(7), C²MADD(14), C²MADD(3), and C²MADD(11). Similarly, for the CMMUL(49) gate we need the C²MADD(4), C²MADD(8), C²MADD(1), and C²MADD(2) gates. The corresponding inverse gates are obtained using extended Euclidean algorithm: $-7^{-1} \equiv 2$, $-14^{-1} \equiv 1$, $-3^{-1} \equiv 8$, $-11^{-1} \equiv 4$, $-4^{-1} \equiv 11$, $-8^{-1} \equiv 13$, $-1^{-1} \equiv 4$, and $-2^{-1} \equiv 7 \pmod{15}$. The resulting gate array is depicted in Fig. 12.

Now we concentrate on the implementation of C²MADD(b) ($1 \leq b \leq N$) gates. Surprisingly, we are considering a special situation: $\log_2(N+1) = \lceil \log_2(N+1) \rceil$. The above equivalence would allow us to simplify the modular adder gate a lot. However, we do not want to take advantage of this special circumstance and thus find the sequence of modules for the C²MADD(b)-operation. The quantum circuit involving three-qubit modules for the modular adder C²MADD(7) is depicted in Fig. 13. Similarly one can construct the sequence of modules for any C²MADD(b) gate. The implementation of the C²MADD(b) gate is constructed of modules discussed in Sec. II. In addition it involves QFT gates for four and five qubits. Their implementations are represented in Fig. 14. Note that the implementation can be optimized further by merging the one-qubit phase-shift gates into adjacent three-qubit gates.

The repetitive execution of the algorithm and measurement of the register $|x\rangle$ yield a distribution of values $k \frac{2^q}{r}$, where r equals the period of the function $7^x \pmod{15}$, k is an positive integer and q is the number of qubits in the register $|x\rangle_q$. If only two qubits are introduced in the register $|x\rangle_2$ the distribution is flat. If the number of qubits q is increased, a peaked distribution appears. In the case of factoring the number 15 the information content of the register $|x\rangle$ remains the same, though. We want to point out that a period of the form 2^k is rare for large N and thus we always have to use the full $2n$ -qubit register $|x\rangle_{2n}$ to ensure that the value of the period can be extracted from the measurement data.

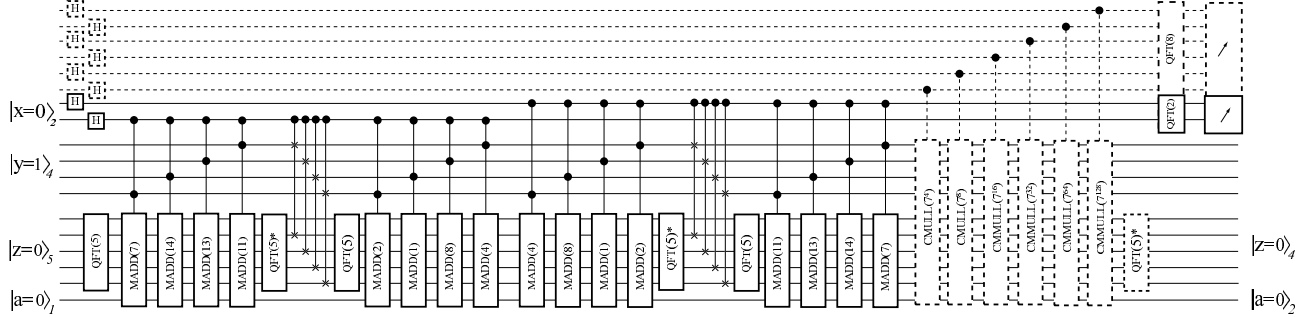


FIG. 12: Quantum circuit for Shor's algorithm for factoring the number 15 with the parameter value $a = 7$. The circuit involves controlled² modular adders, which operate in the Fourier basis. The qubits and operations that would be needed for the full implementation, but omitted in this simplified scheme, are indicated with dashed lines.

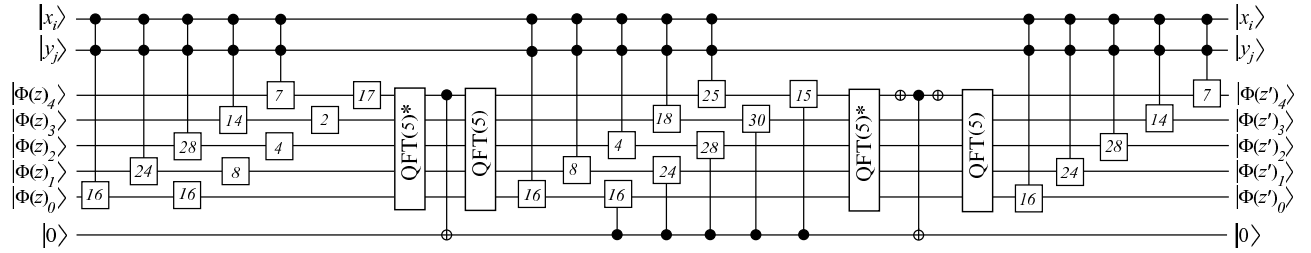


FIG. 13: Decomposition of a controlled² modular adder gate into low-order modules. The gate takes a register $|\Phi(y)\rangle_5$ as an input, which represents the value y in the Fourier basis. The gate is active only if both the two control qubits, $|x_i\rangle$ and $|x_j\rangle$, equal $|1\rangle$. The resulting value $\Phi(y') = \Phi(y + 5 \bmod 15)$ if the gate is active, otherwise $\Phi(y') = \Phi(y)$. The functionality of the gate requires that the input value $y < N \leq 2^4$.

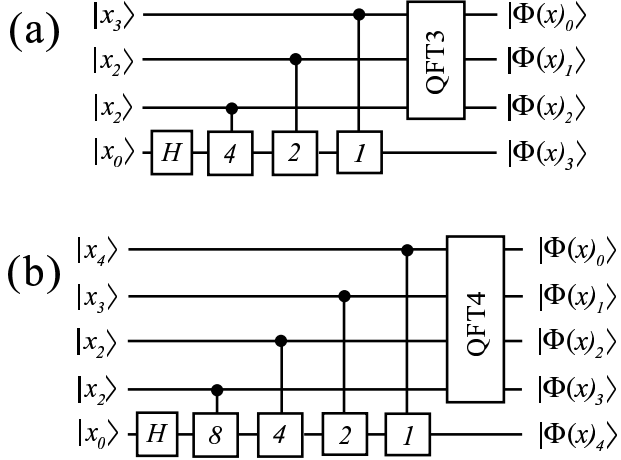


FIG. 14: Quantum Fourier Transformation for (a) four and (b) five qubits. The H stands for the Hadamard gate. The controlled phase shifts are labeled by the numbers k which correspond to phase shifts by $e^{2\pi k i / 2^n}$. Note the reversed order of the qubits on the right-hand side.

B. Physical implementation

The experimental feasibility of the algorithm depends on how complicated it is compared to the present state of technology. Following the above construction of the quantum circuit, the full Shor algorithm to factor 15 requires about 600 three-qubit modules and some 1700 two-qubit modules, in total. If only two-qubit gates are available, about 4900 of them are required. If only a minimal set of elementary gates, say the CNOT gate and one-qubit rotations are available, the total number of gates is remarkably higher. In our scheme the execution time of the algorithm is proportional to the total length of the piecewise linear parameter path which governs the physical implementation of the gate operations. Each of the three-qubit gates requires at least a 13-edged polygonal path $\gamma(t)$ whereas two-qubit gates can be implemented with 5 edges. Consequently, on the order of 15000 edges are required for the whole algorithm if arbitrary three-qubit gates are available, whereas ~ 25000 edges would be required for an implementation with only one- and two-qubit modules.

We discuss the physical implementation of a gate library for Shor's algorithm on a Josephson charge-qubit model through some examples. The quantum circuit involves a number of controlled² modular adders and $\text{QFT}(n)$ gates. The basic building block of the controlled² modular adder is the controlled² phase-shift gate, see Fig. 15. Figure 16 represents the control-parameter sequence for a three-qubit $\text{QFT}(3)$ gate which serves as the foundation for all $\text{QFT}(n)$ gates for $n > 3$. Figure 17 shows how to physically implement the controlled swap gate, which is also required in our implementation. Finally, we have taken advantage of tailored three-qubit implementations: a one-qubit phase-

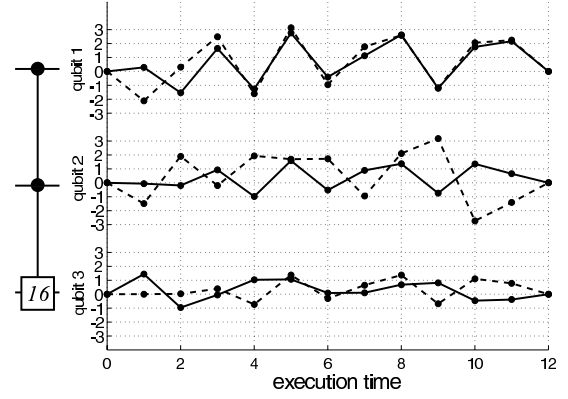


FIG. 15: Control parameters for controlled² phase-shift 16 gate. Solid line indicates B_x^i while the dashed line shows B_z^i .

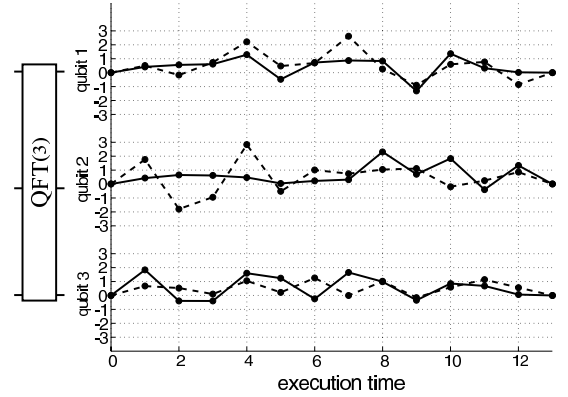


FIG. 16: Control parameters for a three-qubit QFT gate. Solid line indicates B_x^i while the dashed line shows B_z^i .

shift gate and a three-qubit controlled² phase-shift gate are merged into one three-qubit gate, see Fig. 18.

The control parameter sequences presented will yield unitary operations, which approximate the desired gate operations with an accuracy better than 10^{-4} in the error-function values. Since the whole factorization circuit consists of some 10^3 modules, we obtain the total error $\sim 10^{-1}$. This is sufficient for the deduction of the essential information from the output. More classical optimization is required with increasing n . The robustness of the gates obtained was studied numerically by adding Gaussian noise to the vertices of the path. The error function was found to scale linearly with the rms of the variance of the Gaussian noise: error $\approx 6 \times \langle \text{noise} \rangle_{\text{rms}}$, which is probably acceptable.

VI. DISCUSSION

In this paper we have discussed the implementation of Shor's factorization algorithm using a Josephson charge-qubit register. The method is suitable for the first experimental demonstration of factoring a medium-scale integer number $2^4 - 2^{20}$ using Shor's algorithm. For a smaller

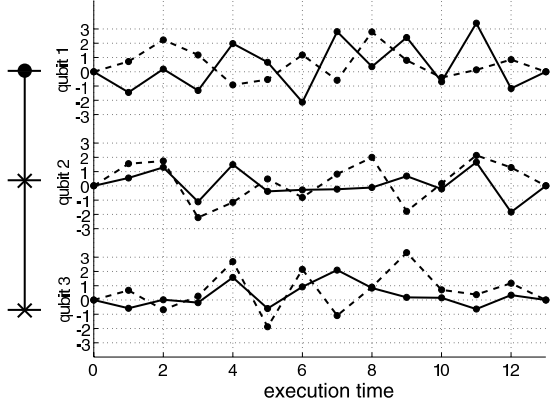


FIG. 17: Control parameters for the Fredkin gate. Solid line indicates B_x^i while the dashed line shows B_z^i .

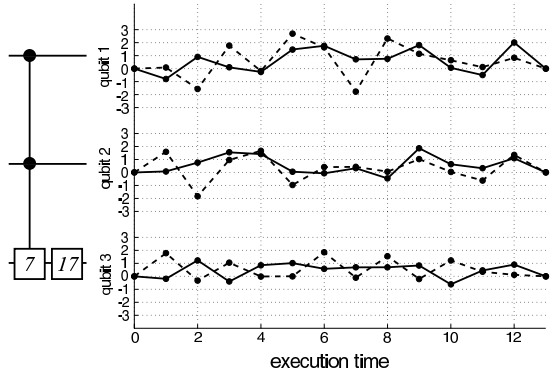


FIG. 18: Control parameters for a composite gate consisting of a controlled² phase-shift and a one-qubit rotation, see text. Solid line indicates B_x^i while the dashed line shows B_z^i .

integer, one should consider more direct methods [3] to implement the modular exponential function. For the large numbers N other approaches, e.g. Schönhage-Strassen multiplication algorithm, will provide a more efficient quantum circuit. Our approach of numerically determining the optimized gates can be generalized to other physical realizations as well. The only requirement is that the system allows total control over the control parameters.

We have found that the number of qubits and quantum gates that are involved in carrying out the algorithm is rather large from the point of view of current technology. Thus the realization of a general factorization algorithm for a large integer N will be challenging. Consequently, the scaling of the chosen algorithm, both in time and space, will be of prime importance.

If a larger number of qubits is available, one could use them to program the parameters a and N of Shor's algorithm into quantum registers, instead of hardwiring them to the quantum-gate sequence. This can be accomplished, for example, by replacing the adders, which add a classical number into a quantum register, by quantum adders [36] which add a quantum register into another

quantum register. This, however, would require two extra registers for the respective parameter values and, furthermore, would yield a longer quantum-gate sequence.

The method we propose utilizes special three-qubit modules, which compress the required quantum-gate array, resulting in a shorter execution time and smaller errors in total. One should also consider other implementations of the quantum algorithms that would employ modules acting on a large number of qubits in order to further decrease the number of gates. This would ease the practical implementation.

The minimization algorithm can be further improved. We expect that a minimization of the path length in the parameter space will provide even shorter parameter sequences than those presented in this paper. We emphasize that the optimization scheme can be modified to produce control-parameter sequences that would be more easily applicable from an experimental point of view. For instance, one can introduce constraints for the optimization to impose limitations for the allowed range of values for the derivatives of the control-parameter field amplitudes. This would ensure that the resulting parameter sequences are experimentally accessible. Furthermore, smooth control-parameter sequences are easily generated by parametrizing the path $\gamma(t)$ using a basis set of analytic functions. Four-qubit (or more) modules may be achievable, but this involves harder numerical optimization.

Finally, let us consider the experimental feasibility of our scheme. To factorize the number 15 we need on the order of 10^4 edges in the control-parameter path. Assuming that the coherence time is on the order of 10^{-6} s implies that the upper limit for the length of each edge is 10^{-10} s. Hence our dimensionless control parameters in the computational examples are on the order of unity, the energy scale in angular frequencies must be at least on the order of 10^{10} s⁻¹. Typical charging energies for, say, thin-film aluminum structures may be on the order of 10^{-23} J which corresponds to 10^{11} s⁻¹. The ultimate limiting energy scale is the BCS gap, which for thin-film aluminum corresponds to an angular frequency of about 3×10^{11} s⁻¹. Based on these rough estimates, we argue that factoring the number 15 on Josephson charge qubits is experimentally reachable, yet extremely hard. Constructing a quantum algorithm to decrypt 512-bit RSA with the scheme that we have presented would require on the order of 2000 qubits and tens of seconds' decoherence time. Error correction might improve the effective coherence time but, on the other hand, it would require more qubits and gates.

We conclude that — with our presented scheme — it is possible to demonstrate the implementation of Shor's algorithm on a Josephson charge-qubit register. Nevertheless, for successful experimental implementation of large-scale algorithms significant improvements in coherence times, fabrication and ultrafast control of qubits is mandatory.

VII. ACKNOWLEDGEMENTS

JJV thanks the Foundation of Technology (TES, Finland) and the Emil Aaltonen Foundation for scholarships. MN thanks the Helsinki University of Technology for a visiting professorship; he is grateful for partial support of a Grant-in-Aid from the Ministry of Education, Culture, Sports, Science, and Technology, Japan (Project

Nos. 14540346 and 13135215); MMS acknowledges the Academy of Finland for a Research Grant in Theoretical Materials Physics. We also thank Robert J. Joynt, Jani Kivioja, Mikko Möttönen, Jukka Pekola and Olli-Matti Penttinen for comments and enlightening discussions. We express our gratitude to CSC - Scientific Computing Ltd (Espoo,Finland) for computing resources.

[1] G. Leuchs and T. Beth (Eds.), *Quantum Information Processing*, WILEY-VCH, Verlag GmbH & Co. KGaA, Weinheim (2003).

[2] M. Steffen, W. van Dam, T. Hogg, G. Breyta, and I. L. Chuang, Phys. Rev. Lett. **90**, 067903 (2003).

[3] L.M.K. Vandersypen, M. Steffen, G. Breyta, C.S. Yannoni, M.H. Sherwood, and I.L. Chuang, Nature **414**, 883 (2001).

[4] D. Leibfried, B. DeMarco, V. Meyer, D. Lucas, M. Barrett, J. Britton, W. M. Itano, B. Jelenkovi, C. Langer, T. Rosenband, and D. J. Wineland, Nature **422**, 412 (2003).

[5] F. Schmidt-Kaler, H. Häffner, M. Riebe, S. Gulde, G. P. T. Lancaster, T. Deuschle, C. Becher, C. F. Roos, J. Eschner, and R. Blatt, Nature **422**, 408 (2003).

[6] C.-P. Yang and S.-I. Chu, Phys. Rev. A **67**, 042311 (2003).

[7] W.G. van der Wiel, S. De Franceschi and J.M. Elzerman, T. Fujisawa, S. Tarucha, and L.P. Kouwenhoven, Rev. Mod. Phys. **75**, 1 (2003).

[8] T. P. Orlando, J. E. Mooij, L. Tian, C. H. van der Wal, L. Levitov, S. Lloyd, and J. J. Mazo, Phys. Rev. B **60**, 15398 (1999).

[9] Y. Yu, S. Han, X. Chu, S. Chu, and Z. Wang, Science **296**, 889 (2002).

[10] Y.A. Pashkin, T. Yamamoto, O. Astafiev, Y. Nakamura, D.V. Averin, J.S. Tsai, Nature **421**, 823 (2003).

[11] Y. Nakamura, Yu. A. Pashkin, and J. S. Tsai, Nature **398**, 786 (1999); Phys. Rev. Lett. **87**, 246601 (2002); Phys. Rev. Lett. **88**, 047901 (2002).

[12] J. M. Martinis, S. Nam, J. Aumentado, and C. Urbina, Phys. Rev. Lett. **89**, 117901 (2002).

[13] D. Vion, A. Aassime, A. Cottet, P. Joyez, H. Pothier, C. Urbina, D. Esteve, and M. H. Devoret, Science **296**, 886 (2002).

[14] J. Q. You, J. S. Tsai, and F. Nori, Phys. Rev. Lett. **89**, 197902 (2002).

[15] D.V. Averin and C. Bruder Phys. Rev. Lett **91**, 057003 (2003).

[16] Yu. Makhlin, G. Schön, and A. Shnirman, Rev. Mod. Phys. **73**, 357 (2001).

[17] A. Barenco, C. H. Bennett, R. Cleve, D. P. DiVincenzo, N. Margolus, P. Shor, T. Sleator, J. Smolin, and H. Weinfurter, Phys. Rev. A **52**, 3457 (1995).

[18] A. V. Aho, R. Sethi, and J. D. Ullman, *Compilers: Principles, Techniques and Tools*, Addison-Wesley, Reading, Massachusetts, (1986).

[19] A.O. Niskanen, J.J. Vartiainen, and M.M. Salomaa, Phys. Rev. Lett **90**, 197901 (2003).

[20] G. Burkard, D. Loss, D. P. DiVincenzo, and J. A. Smolin, Phys. Rev. B **60**, 11404 (1999).

[21] N. Schuch and J. Siewert, Phys. Rev. Lett. **91**, 027902 (2003).

[22] J. Zhang, J. Vala, S. Sastry, and B. Whaley, Phys. Rev. Lett. **91**, 027903 (2003).

[23] P. W. Shor, Proc. 35nd Annual Symposium on Foundations of Computer Science **124**, IEEE Computer Society Press (1994).

[24] L. K. Grover, Phys. Rev. Lett. **79**, 325 (1997).

[25] P. Shor, Phys. Rev. A **52**, 2493 (1995).

[26] A. M. Steane, Phys. Rev. Lett. **77**, 793 (1996).

[27] W.H. Zurek, Rev. Mod. Phys. **75**, 715 (2003).

[28] D. P. DiVincenzo Fortschritte der Physik **48**, 771 (2000).

[29] M Storcz and F. Wilhelm, Phys. Rev. A, **67**, 042319 (2003).

[30] D. R. Stinson, *Cryptography: Theory and Practice*, CRC Press (1995).

[31] F. Bornemann, Notices of the AMS **50**, 545 (2003). M. Agrawal, N. Kayal, and N. Saxena, *PRIMES is in P*, unpublished; http://www.cse.iitk.ac.in/news/primality_v3.pdf;

[32] M. Hirvensalo, *Quantum Computing*, Springer, Berlin (2001).

[33] J. Gruska, *Quantum Computing*, McGraw-Hill, New York (1999).

[34] D. E. Knuth, *The Art of Computer Programming*, Vol. 2: *Seminumerical Algorithms*, third ed., Addison-Wesley, (1998).

[35] S. Beauregard, Quantum Inf. Comput. **3**, 175 (2003).

[36] T. Draper, unpublished, arXiv:quant-ph/008033 (2000).

[37] D. Beckman, A. N. Chari, S. Devabhaktuni, and J. Preskill, Phys. Rev. A **54**, 1034 (1996).

[38] M. A. Nielsen and I.L. Chuang, *Quantum Computation and Quantum Information*, Cambridge University Press, (2000).

[39] M. H. Devoret, *Quantum Fluctuations in Electrical Circuits*, in *Quantum Fluctuations*, S. Reynaud, E. Giacobino, and J. Zinn-Justin, eds., Elsevier Science, B.V. (1997).

[40] V. Vedral, A. Barenco, and A. Ekert, Phys. Rev. A **54**, 147 (1996).

[41] A. O. Niskanen, M. Nakahara, and M. M. Salomaa, Phys. Rev. A **67**, 012319 (2003).

[42] J. C. Lagarias, J. A. Reeds, M. H. Wright, and P. E. Wright, SIAM J. Optim. **9**, 112 (1998).

[43] In the quantum circuit diagrams, we have indicated the size of a register $|x\rangle_m$ with the subscript m .